

# $pp \rightarrow pK^+\Lambda$ reaction in an effective Lagrangian model

R. Shyam

*Saha Institute of Nuclear Physics, Calcutta 700064, India*

*E-mail address: shyam@tnp.saha.ernet.in*

(June 7, 2024)

## Abstract

We investigate the  $pp \rightarrow pK^+\Lambda$  reaction within an effective Lagrangian model where the contributions to the amplitudes are taken into account within the tree level. The initial interaction between the two nucleons is modeled by the exchange of  $\pi$ ,  $\rho$ ,  $\omega$  and  $\sigma$  mesons and the  $\Lambda K^+$  production proceeds via the excitation of the  $N^*(1650)$ ,  $N^*(1710)$ ,  $N^*(1720)$  baryonic resonances. The parameters of the model at the nucleon-nucleon-meson vertices are determined by fitting the elastic nucleon-nucleon scattering with an effective interaction based on the exchange of these four mesons, while those at the resonance vertices are calculated from the known decay widths of the resonances as well as the vector meson dominance model. Available experimental data is described well by this approach. The one-pion-exchange diagram dominates the production process at both higher and lower beam energies. The  $\rho$  and  $\omega$  meson exchanges make negligible contributions. However, the  $\sigma$ -exchange processes contribute substantially to the total cross sections at lower beam energies. The excitation of the  $N^*(1710)$  and  $N^*(1650)$  resonances dominate this reaction at beam momenta above and below 3 GeV/c respectively. The interference among the amplitudes of various resonance excitation processes is significant. For beam energies very close to the  $K^+$  production threshold the hyperon-proton final state interaction effects are quite important. The data is selective about the model used to describe the low energy scattering of the two final state baryons.

PACS numbers: 13.60.Le, 13.75.Cs, 11.80.-m, 12.40.Vv

KEYWORD:  $K^+$  production in  $pp$  collisions, effective Lagrangian model, contribution of meson exchanges and baryonic resonances.

Typeset using REVTeX

## I. INTRODUCTION

In recent years there has been a considerable amount of interest in the study of the associated production reaction  $p + p \rightarrow p + K^+ + \Lambda$ . This is expected to provide information on the manifestation of quantum chromodynamics (QCD) in the non-perturbative regime larger than that of the low energy pion physics where the low energy theorems and partial conservation of axial current (PCAC) constraints provide a useful insight into the relevant physics [1]. The strangeness quantum number introduced by this reaction leads to new degrees of freedom into this domain which are expected to probe the admixture of  $\bar{s}s$  quark pairs in the nucleon wave function [2] and also the hyperon-nucleon and hyperon-strange meson interactions [3,4].

The elementary proton-proton-strange meson production cross sections are the most important ingredients in the transport model studies of the  $K^+$ -meson production in the nucleus-nucleus collisions, which provide information on not only the initial collision dynamics but also the nuclear equation of state at high density [5–12]. Furthermore, the enhancement in the strangeness production has been proposed as a signature for the formation of the quark-gluon plasma in high energy nucleus-nucleus collisions [13,14].

The experimental data on the  $pp \rightarrow pK^+\Lambda$  reaction is very scarce. The measurements performed in late 1960s and 1970s provide total cross sections for this reaction at beam momenta greater than 2.80 GeV/c (see e.g. [15]). With the advent of the high-duty proton-synchrotron COSY at the Forschungszentrum, Jülich, it has become possible to perform systematic studies of the associated strangeness production at beam momenta very close to the reaction threshold (2.340 GeV/c). The first round of experiments at COSY have already added [16] 10 new data points to the data base. At near threshold beam energies the final state interaction among the outgoing particles is significant. Therefore, the new set of data are expected to probe also the hyperon-nucleon and hyperon-strange meson interactions along with the mechanism of the strangeness production in proton-proton collisions.

The existing theoretical studies of this reaction are based either on a single boson ( $\pi$  or  $K$  meson) exchange mechanism [17–20] or a resonance model [22–24]. In the first method, the  $K^+$  production is assumed to take place essentially through the exchange of one intermediate pion or  $K$ -meson; the excitation of any intermediate nucleon resonance is not considered. The  $K$ -meson exchange amplitudes were found to dominate [17,20] the production cross sections. However, the relative sign of the pion and  $K$ -meson exchange amplitudes were not fixed in this approach [20]. Furthermore, it has been argued that the existing high energy data can be well reproduced considering only the single pion-exchange process [18,19] since the contribution of the  $K$ -meson exchange amplitude can be compensated by various parameters of the model.

In the resonance model [21] of the strangeness production in  $pp$  collisions, the  $\pi$ ,  $\eta$ , and  $\rho$ -meson exchanges are included and the  $K^+$  meson production proceeds through the excitation of the  $N^*(1650)$ ,  $N^*(1710)$  and  $N^*(1720)$  resonances [22,24]. However, the terms in the total amplitude involving the interference of various resonances is neglected in these calculations. Moreover, the parameters of the  $NN\pi$  and  $NN\rho$  vertices were taken from the Bonn nucleon-nucleon potential which may not be adequate at higher beam energies as these have been determined by fitting the  $NN$  scattering data below the  $NN\pi$  production threshold. At the same time, the finite life-time of the  $\rho$  meson has not been taken into

account while calculating the relevant coupling constants from the experimental branching ratios.

In this paper, we investigate the associated  $K^+$  production in the proton-proton collisions in the framework of an effective Lagrangian approach [25–28], following and extending our previous study [29,30] on  $\pi^0$  and  $\pi^+$  production. Initial interaction between two incoming nucleons is modeled by an effective Lagrangian which is based on the exchange of the  $\pi$ ,  $\rho$ ,  $\omega$  and  $\sigma$  mesons. The coupling constants at the nucleon-nucleon-meson vertices are determined by directly fitting the T-matrices of the nucleon-nucleon ( $NN$ ) scattering in the relevant energy region [32]. The effective-Lagrangian uses the pseudovector (PV) coupling for the nucleon-nucleon-pion vertex (unlike the resonance model [22]), and thus incorporates the low energy theorems [33] of current algebra and the hypothesis of partially conserved axial-vector current (PCAC). The  $K^+$  production proceeds via excitation of the  $N^*(1650)$ ,  $N^*(1710)$  and  $N^*(1720)$  intermediate baryonic resonance states which have appreciable branching ratios for the decay into the  $K^+\Lambda$  channel. The interference terms between various intermediate resonance states are included which marks a major difference between our work and the resonance model [22]. To describe the recent near threshold data, the final state interaction between the outgoing particles is included within the framework of the Watson-Migdal theory [30].

The remainder of this paper is organized in the following way. Section II contains details of our theoretical approach. Section III comprises the results of our analysis and their critical discussion. The summary and conclusions of our work is presented in section IV. Finally some technical details are given in appendix A.

## II. FORMALISM

We consider the tree-level structure (Fig. 1) of the amplitudes for the associated  $K^+\Lambda$  production in proton-proton collisions, which proceeds via excitation of the  $N^*(1650)(\frac{1}{2}^-)$ ,  $N^*(1710)(\frac{1}{2}^+)$  and  $N^*(1720)(\frac{3}{2}^+)$  intermediate resonances. To evaluate these amplitudes within the effective Lagrangian approach, one needs to know the effective Lagrangians (and the coupling constants appearing therein) at (i) nucleon-nucleon-meson, (ii) resonance-nucleon-meson, and (iii) resonance- $K^+$ -hyperon vertices. These are discussed in the following subsections.

### A. Nucleon-nucleon-meson vertex

The parameters for  $NN$  vertices are determined by fitting the  $NN$  elastic scattering T matrix with an effective  $NN$  interaction based on the  $\pi$ ,  $\rho$ ,  $\omega$  and  $\sigma$  meson exchanges. The effective meson- $NN$  Lagrangians are

$$\mathcal{L}_{NN\pi} = -\frac{g_{NN\pi}}{2m_N} \bar{\Psi}_N \gamma_5 \gamma_\mu \boldsymbol{\tau} \cdot (\partial^\mu \boldsymbol{\Phi}_\pi) \Psi_N. \quad (1)$$

$$\mathcal{L}_{NN\rho} = -g_{NN\rho} \bar{\Psi}_N \left( \gamma_\mu + \frac{k_\rho}{2m_N} \sigma_{\mu\nu} \partial^\nu \right) \boldsymbol{\tau} \cdot \boldsymbol{\rho}^\mu \Psi_N. \quad (2)$$

$$\mathcal{L}_{NN\omega} = -g_{NN\omega}\bar{\Psi}_N\left(\gamma_\mu + \frac{k_\omega}{2m_N}\sigma_{\mu\nu}\partial^\nu\right)\omega^\mu\Psi_N. \quad (3)$$

$$\mathcal{L}_{NN\sigma} = g_{NN\sigma}\bar{\Psi}_N\sigma\Psi_N. \quad (4)$$

In Eqs. (2) - (3)  $\sigma_{\mu\nu}$  is defined as

$$\sigma_{\mu\nu} = \frac{i}{2}(\gamma_\mu\gamma_\nu - \gamma_\nu\gamma_\mu) \quad (5)$$

We have used the notations and conventions of Bjorken and Drell [31]. In Eq. (1)  $m_N$  denotes the nucleon mass. It should be noted that we have used a PV coupling for the  $NN\pi$  vertex. Since we use these Lagrangians to directly model the T-matrix, we have also included a nucleon-nucleon-axial-vector-isovector vertex, with the effective Lagrangian given by

$$\mathcal{L}_{NNA} = g_{NNA}\bar{\Psi}\gamma_5\gamma_\mu\boldsymbol{\tau}\Psi \cdot \mathbf{A}^\mu, \quad (6)$$

where  $A$  represents the axial-vector meson field. This term is introduced because in the limit of large axial meson mass ( $m_A$ ) it cures the unphysical behavior in the angular distribution of  $NN$  scattering caused by the contact term in the one-pion exchange amplitude [32], if  $g_{NNA}$  is chosen to be

$$g_{NNA} = \frac{1}{\sqrt{3}}m_A\left(\frac{f_\pi}{m_\pi}\right). \quad (7)$$

with very large ( $\gg m_N$ )  $m_A$ .

We introduce, at each interaction vertex, the form factor

$$F_i^{NN} = \left(\frac{\lambda_i^2 - m_i^2}{\lambda_i^2 - q_i^2}\right), i = \pi, \rho, \sigma, \omega, \quad (8)$$

where  $q$  is the four momentum and  $m$  the mass of the exchanged meson. The form factors suppress the contributions of high momenta and the parameter  $\lambda$ , which governs the range of suppression, can be related to the hadron size. Since  $NN$  elastic scattering cross sections decrease gradually with the beam energy (beyond certain value), we take energy dependent meson-nucleon coupling constants of the following form

$$g(\sqrt{s}) = g_0\exp(-\ell\sqrt{s}), \quad (9)$$

in order to reproduce these data in the entire range of beam energies. The parameters,  $g_0$ ,  $\lambda$  and  $\ell$  were determined by fitting to the elastic proton-proton and proton-neutron scattering data at the beam energies in the range of 400 MeV to 4.0 GeV [29,32]. The values of various parameters are shown in Table 1, which are the same as those used in the calculations of the pion production in proton-proton collisions [29,30]. In this way we ensure that the  $NN$  elastic scattering channel remains the same in the description of various inelastic channels within this approach, as it should be.

## B. Resonance-nucleon-meson vertex

Since the  $\Lambda$ -hyperon has zero isospin, only isospin-1/2 nucleon resonances are allowed. Below 2 GeV center of mass (c.m.) energy, only three resonances have significant decay branching ratios into  $K^+\Lambda$  channel; these are the  $N^*(1650)$ ,  $N^*(1710)$ , and  $N^*(1720)$  resonances with the respective  $K^+\Lambda$  branching ratios being 3-11%, 5-25% and 1-15% [34]. In this work only these three resonances have been considered. The  $N^*(1700)$  resonance having very small (and uncertain) branching ratio for the decay to this channel has been excluded.

Since all the three resonances can couple to the meson-nucleon channel considered in the previous section, we require the effective Lagrangians for all the four resonance-nucleon-meson vertices corresponding to all the included resonances. For the coupling of the spin-1/2- resonances to pion we again have the choice of PS or PV couplings. The corresponding effective Lagrangians can be written as [28,35]

$$\mathcal{L}_{N_{1/2}^*N\pi}^{PV} = -\frac{g_{N_{1/2}^*N\pi}}{M}\bar{\Psi}_{N^*}\Gamma_\mu\boldsymbol{\tau}\cdot(\partial^\mu\boldsymbol{\Phi}_\pi)\Psi_N + \text{h.c.} \quad (10)$$

$$\mathcal{L}_{N_{1/2}^*N\pi}^{PS} = -g_{N_{1/2}^*N\pi}\bar{\Psi}_{N^*}i\Gamma\boldsymbol{\tau}\boldsymbol{\Phi}_\pi\Psi_N + \text{h.c.}, \quad (11)$$

where  $M = (m_{N^*} \pm m_N)$ , with the upper sign for even parity and lower sign for odd parity resonance. The operators  $\Gamma, \Gamma_\mu$ , are given by,

$$\Gamma = \gamma_5, \quad \Gamma_\mu = \gamma_5\gamma_\mu, \quad (12)$$

$$\Gamma = 1, \quad \Gamma_\mu = \gamma_\mu, \quad (13)$$

for resonances of even and odd parities, respectively. We have performed calculations with both of these couplings. The effective Lagrangians for the coupling of resonances to other mesons are similar to those given by Eq. (2)-(4),

$$\mathcal{L}_{N_{1/2}^*N\rho} = -g_{N_{1/2}^*N\rho}\bar{\Psi}_{N^*}\frac{1}{2m_N}\Gamma_{\mu\nu}\partial^\nu\boldsymbol{\tau}\cdot\boldsymbol{\rho}^\mu\Psi_N + \text{h.c.} \quad (14)$$

$$\mathcal{L}_{N_{1/2}^*N\omega} = -g_{N_{1/2}^*N\omega}\bar{\Psi}_{N^*}\frac{1}{2m_N}\Gamma_{\mu\nu}\partial^\nu\omega^\mu\Psi_N + \text{h.c.} \quad (15)$$

$$\mathcal{L}_{N_{1/2}^*N\sigma} = g_{N_{1/2}^*N\sigma}\bar{\Psi}_{N^*}\Gamma'\sigma\Psi_N + \text{h.c.}, \quad (16)$$

The operators  $\Gamma'$  and  $\Gamma_{\mu\nu}$  are given by,

$$\Gamma' = 1, \quad \Gamma_{\mu\nu} = \sigma_{\mu\nu} \quad (17)$$

$$\Gamma' = \gamma_5, \quad \Gamma_{\mu\nu} = \gamma_5\sigma_{\mu\nu} \quad (18)$$

for resonances of even and odd parities, respectively.

The even parity isospin-1/2  $N^*(1720)$  resonance is a spin-3/2 nucleon excited state. We have used the following effective Lagrangians for vertices involving this resonance [28,35]

$$\mathcal{L}_{N^*N\pi} = \frac{g_{N_{3/2}^*N\pi}}{m_\pi}\bar{\Psi}_\mu\boldsymbol{\tau}\cdot\partial^\mu\boldsymbol{\Phi}_\pi\Psi_N + \text{h.c.} \quad (19)$$

$$\mathcal{L}_{N^*N\rho} = i\frac{g_{N_{3/2}^*N\rho}}{m_{N^*} + m_N}\bar{\Psi}_\mu\boldsymbol{\tau}(\partial^\nu\boldsymbol{\rho}^\mu - \partial^\mu\boldsymbol{\rho}^\nu)\gamma_\nu\gamma_5\Psi_N + \text{h.c.} \quad (20)$$

$$\mathcal{L}_{N^*N\omega} = i \frac{g_{N_{3/2}^*N\omega}}{m_{N^*} + m_N} \bar{\Psi}_\mu \boldsymbol{\tau} (\partial^\nu \omega^\mu - \partial^\mu \omega^\nu) \gamma_\nu \gamma_5 \Psi_N + \text{h.c.} \quad (21)$$

$$\mathcal{L}_{N^*N\sigma} = \frac{g_{N_{3/2}^*N\sigma}}{m_\sigma} \bar{\Psi}_\mu \boldsymbol{\tau} \cdot (\partial^\mu \sigma) \Psi_N + \text{h.c.} \quad (22)$$

Here,  $\bar{\Psi}_\mu$  is the  $N^*(1720)$  vector spinor. It should be remarked here that an operator  $\Theta_{\alpha\mu}(z) = g_{\alpha\nu} - \frac{1}{2}(1+2z)\gamma_\alpha\gamma_\mu$  has also been included in the vector spinor vertex in Refs. [28,35]. This operator describes the off-shell admixture of the spin-1/2 fields [36]. The choice of the off-shell parameter  $z$  is arbitrary and it is treated as a free parameter to be determined by fitting to the data. This operator can be easily introduced in Eqs. (15)-(18) which will introduce four additional free parameter in our calculations. We however, work with the Lagrangians as given in Eqs. (19)-(22), which are identical to those given in [28,35] for  $z = 0.5$ .

### C. Resonance-hyperon-strange meson vertex

For vertices involving spin-1/2 resonances, there is again the PS and PV coupling option. In principle one can select a linear combination of both and fit the PS/PV ratio to the data. However, to minimize the number of parameters we choose either PS or PV couplings at a time. The effective Lagrangians for the  $N^*\Lambda K^+$  vertex is written in the following way,

For spin-1/2 resonance,

$$\mathcal{L}_{N_{1/2}^*\Lambda K^+}^{PV} = -\frac{g_{N_{1/2}^*\Lambda K^+}}{M'} \bar{\Psi}_{N^*} \Gamma_\mu \boldsymbol{\tau} \cdot (\partial^\mu \Phi_{K^+}) \Psi_N + \text{h.c.}, \quad (23)$$

$$\mathcal{L}_{N_{1/2}^*\Lambda K^+}^{PS} = -g_{N_{1/2}^*\Lambda K^+} \bar{\Psi}_{N^*} i \Gamma \boldsymbol{\tau} \Phi_{K^+} \Psi_N + \text{h.c.}, \quad (24)$$

where  $M' = m_{N^*} \pm m_\Lambda$ , with the upper sign for even parity and lower sign for odd parity resonance.

For spin-3/2 resonance,

$$\mathcal{L}_{N_{3/2}^*\Lambda K^+} = \frac{g_{N_{3/2}^*\Lambda K^+}}{m_{K^+}} \bar{\Psi}_\mu \boldsymbol{\tau} \cdot \partial^\mu \Phi_{K^+} \Psi_N + \text{h.c.} \quad (25)$$

### D. Coupling constant for resonances

The resonance couplings are determined from the experimentally observed quantities such as the branching ratios for the decay of the resonances to the corresponding channels.

The partial width for the decay of a resonance (in its rest frame) of mass  $M_{N^*}$  into a meson of mass  $m_m$  and energy  $E_m$  and a nucleon is written in terms of the Lorentz invariant matrix element  $\mathcal{M}$  as

$$d\Gamma = \frac{(2\pi)^4}{2M_{N^*}} |\mathcal{M}|^2 \delta^4(P_{N^*} - p_m - p_N) \frac{d^3 p_m}{(2\pi)^3 2E_m} \frac{m_N}{E_N} \frac{d^3 p_N}{(2\pi)^3}, \quad (26)$$

In case of the meson (in the decay channel) having a finite life time for the decay to another channel (e.g  $\rho \rightarrow \pi\pi$ ), an integration over the phase-space for this decay must be included [37–39].

**(i).  $N^*N\pi$  vertex**

For the spin-1/2 resonance the  $N^*N\pi$  decay width, with the PS coupling, is given by

$$\Gamma_{N^*_{1/2}N\pi} = \frac{3}{4\pi} g_{N^*_{1/2}N\pi}^2 \frac{E_N \pm m_N}{m_{N^*}} p_\pi^{cm}, \quad (27)$$

while that with the corresponding PV coupling is

$$\Gamma_{N^*_{1/2}N\pi} = \frac{3}{4\pi} \left( \frac{g_{N^*_{1/2}N\pi}}{M} \right)^2 \left[ \frac{2E_\pi(E_N E_\pi + (p_\pi^{cm})^2) - m_\pi^2(E_N \pm m_N)}{m_{N^*}} \right] p_\pi^{cm}. \quad (28)$$

where

$$p_\pi^{cm} = \frac{[m_{N^*}^2 - (m_N + m_\pi)^2][m_{N^*}^2 - (m_N - m_\pi)^2]}{4m_{N^*}^2}, \quad (29)$$

$$E_N = \sqrt{(p_\pi^{cm})^2 + m_N^2}, \quad (30)$$

$$E_\pi = \sqrt{(p_\pi^{cm})^2 + m_\pi^2}. \quad (31)$$

For spin-3/2 resonance the  $N^*N\pi$  decay width is

$$\Gamma_{N^*_{3/2}N\pi} = \frac{1}{12\pi} \left( \frac{g_{N^*_{3/2}N\pi}}{m_\pi} \right)^2 \frac{E_N \pm m_N}{m_{N^*}} (p_\pi^{cm})^3 \quad (32)$$

The plus and minus sign in Eqs (27) corresponds to odd and even parity resonances respectively, while in Eqs. (28) and (32) the situation is reversed.

**(ii).  $N^*N\rho$  vertex**

The partial decay width of each resonance for the decay into nucleon and two pions via the  $\rho$  meson is given by

$$\Gamma(m_{N^*}) = 2 \int_{2m_\pi}^{m_{N^*} - m_N} dm m \Gamma^*(m) S(m). \quad (33)$$

In this equation the spectral function  $S(m)$  is defined as,

$$S(m) = -\frac{1}{\pi} \text{Im} D_\rho(m), \quad (34)$$

where

$$D_\rho(m) = \frac{1}{m^2 - m_\rho^2 + im\Gamma_{\rho \rightarrow \pi\pi}}, \quad (35)$$

with

$$\Gamma_{\rho \rightarrow \pi\pi} = \Gamma_{\rho \rightarrow \pi\pi}^0 \frac{m_\rho^2}{m^2} \left[ \frac{p_{\rho\pi\pi}(m)}{p_{\rho\pi\pi}(m_\rho)} \right]^3. \quad (36)$$

The value of  $\Gamma_{\rho \rightarrow \pi\pi}^0$  is taken to be 150 MeV. The  $\rho \rightarrow \pi\pi$  decay four-momenta  $p_{\rho\pi\pi}$  are defined as

$$p_{\rho\pi\pi}(m) = \frac{[m^2 - 4m_\pi^2][m^2]}{4m^2}. \quad (37)$$

In Eq. (33)  $\Gamma^*(m)$  is defined in the following way,

For spin-1/2 even parity resonance

$$\Gamma^*(m) = \frac{1}{4\pi} \left( \frac{g_{N_{1/2}^* N \rho}}{2m_N} \right)^2 \left[ \frac{4(E_N^* + E_m)(p_m^{cm})^2 + 3(E_N^* - m_N)m^2}{m_{N^*}} \right] p_m^{cm}, \quad (38)$$

$$E_N^* = \sqrt{(p_m^{cm})^2 + m_N^2}, \quad (39)$$

$$E_m = \sqrt{(p_m^{cm})^2 + m^2}, \quad (40)$$

where  $p_m^{cm}$  is given in the same way as Eq. (29) with  $m_\pi$  replaced by  $m$ .

For spin-1/2 odd parity resonance

$$\Gamma^*(m) = \frac{1}{4\pi} \left( \frac{g_{N_{1/2}^* N \rho}}{2m_N} \right)^2 \left[ \frac{-4(E_N^* + E_m)(p_m^{cm})^2 - 3(E_N^* + m_N)m^2}{m_{N^*}} \right] p_m^{cm}. \quad (41)$$

For spin-3/2 even parity resonance

$$\Gamma^*(m) = \frac{1}{12\pi} \left( \frac{g_{N_{3/2}^* N \rho}}{m_{N^*} + m_N} \right)^2 \left[ \frac{2(2E_N^* + E_m)(p_m^{cm})^2 + 3(E_N^* - m_N)m^2}{m_{N^*}} \right] p_m^{cm}. \quad (42)$$

### (iii). $N^*N\omega$ vertex

Since the resonances considered in this study have no known branching ratios for the decay into the  $N\omega$  channel, we determine the coupling constants for the  $N^*N\omega$  vertices by the strict vector meson dominance (VMD) hypothesis [40], which is based essentially on the assumption that the coupling of photons on hadrons takes place through a vector meson.

The  $N^*N\gamma$  partial widths are given as following:

For spin-1/2 even parity resonance,

$$\Gamma_{N^*N\gamma} = \frac{1}{\pi} \frac{m_N}{m_{N^*}} (\mu_{N^*})^2 (q_f^3) \quad (43)$$

For spin-1/2 odd parity resonance,

$$\Gamma_{N^*N\gamma} = \frac{3}{2} \frac{m_N}{m_{N^*}} (\mu_{N^*})^2 (m^2 + q_f^2) q_f \quad (44)$$

For spin-3/2 even parity resonance,

$$\Gamma_{N^*N\gamma} = \frac{1}{\pi} \frac{m_N}{m_{N^*}} (\mu_{N^*})^2 (q_f^3) \quad (45)$$

In these equations,  $q_f = ((m_{N^*}^2 - m_N^2)/2m_{N^*})$ . The value of  $\mu_{N^*}$  is determined by fitting to the  $N\gamma$  partial width of each resonance which is given in terms of the helicity amplitudes  $A_{1/2}$  and  $A_{3/2}$  by [34]



$$\Gamma_\gamma = \frac{q_f^2}{\pi} \frac{2m_N}{(2J+1)m_{N^*}} \left[ |A_{1/2}|^2 + |A_{3/2}|^2 \right], \quad (46)$$

where  $J$  is the resonance spin.  $\mu_{N^*}$  is written as the ratio of the couplings at  $N^*\omega$  and  $\omega\gamma$  vertices as

$$\mu_{N^*} = \frac{eg_{N^*\omega}}{g_{\omega\gamma}} \quad (47)$$

Using above equations together with the experimental helicity amplitudes the values of the coupling constants for the  $N^*N\omega$  vertices can be determined. We have used  $g_{\omega\gamma} = 17$  in our calculations.

**(iv).  $N^*N\sigma$  vertex**

As the sigma meson is, most of the time, a resonance of two pions [41] in the S-state, the coupling constants for the  $N^*N\sigma$  vertices are determined from the branching ratios of the decay of the resonances into two pions. We, however, reduce the experimental values of these ratios by two third to account for the fact that this correlated state provides only about 2/3 of the total  $2\pi$ -exchange. The expressions for the partial widths are similar to those given by Eqs. (27)-(32).

**(iv).  $N^*\Lambda K^+$  vertex**

The coupling constants for the  $N^*\Lambda K^+$  vertex are determined from the experimental branching ratios for the  $N^* \rightarrow \Lambda K^+$  decay. The expressions for the decay widths are similar to those given by Eqs. (27) - (32).

We assume that the off-shell dependence of the  $NN^*$  vertices are determined solely by multiplying the vertex constants by the form factors, which have the dipole form [29,42]

$$F_i^{NN^*} = \left( \frac{(\lambda_i^{N^*})^2 - m_i^2}{(\lambda_i^{N^*})^2 - q_i^2} \right)^2, \quad i = \pi, \rho, \sigma, \omega, \quad (48)$$

The resonance properties used in the calculations of the decay widths are given in Table 2, where the resulting coupling constants and the adopted values of the cut-off parameters ( $\lambda_i^{N^*}$ ) are also given. It may be noted that we have fixed the latter to one value in order to minimize the number of free parameters.

## E. Propagators

We require the propagators for various mesons and nucleon resonances in the calculation of the amplitudes. The propagators for pion,  $\rho$  meson and axial-vector mesons are given by

$$G_\pi(q) = \frac{i}{(q^2 - m_\pi^2)} \quad (49)$$

$$G_\rho^{\mu\nu}(q) = -i \left( \frac{g^{\mu\nu} - q^\mu q^\nu / q^2}{q^2 - m_\rho^2} \right) \quad (50)$$

$$G_A^{\mu\nu}(q) = -i \left( \frac{g^{\mu\nu}}{q^2 - m_A^2} \right) \quad (51)$$

In Eq. (51), the mass of the axial meson is taken to be very large (188 GeV), as the corresponding amplitude is that of the contact term. The propagators for  $\omega$  and  $\sigma$  mesons are similar to those given by Eqs. (50) and (49) respectively.

The propagators for spin-1/2 and spin-3/2 resonances are

$$G_{N_{1/2}^*}(p) = i \left( \frac{p_\eta \gamma^\eta + m_{N_{1/2}^*}}{p^2 - (m_{N_{1/2}^*} - i(\Gamma_{N_{1/2}^*}/2))^2} \right), \quad (52)$$

$$G_{N_{3/2}^*}^{\mu\nu}(p) = -\frac{i(\not{p} + m_{N_{3/2}^*})}{p^2 - (m_{N_{3/2}^*} - i(\Gamma_{N_{3/2}^*}/2))^2} \times [g^{\mu\nu} - \frac{1}{3}\gamma^\mu\gamma^\nu - \frac{2}{3m_{N_{3/2}^*}^2}p^\mu p^\nu + \frac{1}{3m_{N_{3/2}^*}^2}(p^\mu\gamma^\nu - p^\nu\gamma^\mu)]. \quad (53)$$

In Eqs. (52) - (53),  $\Gamma_{N^*}^*$  is the total width of the resonance which is introduced in the denominator term ( $p^2 - m_{N^*}^2$ ) to account for the fact that the resonances are not the stable particles; they have a finite life time for the decay into various channels.  $\Gamma_{N^*}$  is a function of the center of mass momentum of the decay channel, and it is taken to be the sum of the widths for pion and rho decay (the other decay channels are considered only implicitly by adding their branching ratios to that of the pion channel)

$$\Gamma_{N^*} = \Gamma_{N^* \rightarrow N\pi} + \Gamma_{N^* \rightarrow N\rho} \quad (54)$$

$\Gamma_{N^* \rightarrow N\rho}$  is calculated according to Eq. (33).  $\Gamma_{N^* \rightarrow N\pi}$  is taken to be

$$\Gamma_{N^* \rightarrow N\pi} = \Gamma_0 \left( \frac{p_{\pi R}^{cm}}{p_\pi^{cm}} \right)^{2\ell+1}, \quad (55)$$

where  $\ell$  is the orbital angular momentum of the resonance.  $p_\pi^{cm}$  is as defined in Eq. (28) and  $p_{\pi R}^{cm}$  is given by the same equation with  $m_{N^*}$  replaced by  $p$  of Eqs. (52) - (53).  $\Gamma_0$  is taken to be the total on-shell width of the resonance minus the corresponding width for the nucleon- $\rho$  meson decay channel.

## F. Amplitudes and cross sections

After having established the effective Lagrangians, coupling constants and form of the propagators, we can now proceed to calculate the amplitudes for various diagrams associated with the  $pp \rightarrow p\Lambda K^+$  reaction. These amplitudes can be written by following the well known Feynman rules [43]. The isospin part is treated separately. This gives rise to a constant factor for each graph, which is unity for the reaction under study.

In the following we give expressions for various amplitudes for one graph only, ( we use the PV couplings for the  $N^*\Lambda K^+$  vertices involving spin-1/2 resonances of even and odd parities ). It is straight-forward to write the amplitudes for the rest of the cases.

### Pion exchange and $N^*(1710)$ excitation

*PV Coupling for  $N^*N\pi$  vertex*

$$M_{N_{1/2}^*}^\pi = - \left( \frac{g_{NN\pi}}{2m_N} \right) \left( \frac{g_{N_{1/2}^* N\pi}}{m_{N_{1/2}^*} + m_N} \right) \left( \frac{g_{N_{1/2}^* \Lambda K^+}}{m_{N_{1/2}^*} + m_\Lambda} \right) \\ \times \bar{\psi}(p_\Lambda) \gamma_5 \gamma_\delta p_{K^+}^\delta G_{N_{1/2}^*}(p) \gamma_5 \gamma_\mu q^\mu \psi(p_1) G_\pi(q) \psi(p_3) \gamma_5 \gamma_\nu q^\nu \psi(p_2). \quad (56)$$

*PS Coupling for  $N^* N \pi$  vertex*

$$M_{N_{1/2}^*}^\pi = - \left( \frac{g_{NN\pi}}{2m_N} \right) g_{N_{1/2}^* N\pi} \left( \frac{g_{N_{1/2}^* \Lambda K^+}}{m_{N_{1/2}^*} + m_\Lambda} \right) \\ \times \bar{\psi}(p_\Lambda) \gamma_5 \gamma_\mu p_{K^+}^\mu G_{N_{1/2}^*}(p) \gamma_5 \psi(p_1) G_\pi(q) \bar{\psi}(p_3) \gamma_5 \gamma_\nu q^\nu \psi(p_2). \quad (57)$$

In Eq.(56) and (57),  $G$  are the propagators as defined above.  $p_1$  and  $p_2$  are the momenta of the protons in the entrance channel (the one on the left having suffix 1),  $p_\Lambda$  and  $p_3$  are the momenta of the hyperon and the proton in the final channel. The intermediate momenta are given by  $q = p_2 - p_3$  and  $p = p_{K^+} + p_\Lambda$ .  $\psi$  is the Dirac spinor in the spin space.

**$\rho$  meson exchange and  $N^*(1710)$  excitation**

$$M_{N_{1/2}^*}^\rho = -g_{NN\rho} g_{N_{1/2}^* N\rho} \left( \frac{g_{N_{1/2}^* \Lambda K^+}}{m_{N_{1/2}^*} + m_\Lambda} \right) \bar{\psi}(p_\Lambda) \gamma_5 \gamma_\delta p_{K^+}^\delta G_{N_{1/2}^*}(p) \frac{i\sigma_{\alpha\beta}}{2m_N} q^\beta \psi(p_1) \\ \times G_\rho^{\mu\alpha}(q) \bar{\psi}(p_3) \left( \gamma_\mu + \frac{ik_\rho}{2m_N} \sigma_{\nu\mu} q^\nu \right) \psi(p_2). \quad (58)$$

**$\omega$  meson exchange and  $N^*(1710)$  excitation**

In this case the form of the amplitude is similar to that of the  $\rho$  meson exchange (Eq. (58)).

**$\sigma$  meson exchange and  $N^*(1710)$  excitation**

$$M_{N_{1/2}^*}^\sigma = -g_{NN\sigma} g_{N_{1/2}^* N\sigma} \left( \frac{g_{N_{1/2}^* \Lambda K^+}}{m_{N_{1/2}^*} + m_\Lambda} \right) \bar{\psi}(p_\Lambda) \gamma_5 \gamma_\delta p_{K^+}^\delta G_{N_{1/2}^*}(p) \psi(p_1) \\ \times G_\sigma(q) \bar{\psi}(p_3) \psi(p_2). \quad (59)$$

**Heavy axial meson exchange and  $N^*(1710)$  excitation**

$$M_{N_{1/2}^*}^A = -g_{NNA} g_{N_{1/2}^* NA} \left( \frac{g_{N_{1/2}^* \Lambda K^+}}{m_{N_{1/2}^*} + m_\Lambda} \right) \bar{\psi}(p_\Lambda) \gamma_5 \gamma_\delta p_{K^+}^\delta G_{N_{1/2}^*}(p) \gamma_5 \gamma_\mu \psi(p_1) \\ \times G_A^{\mu\nu}(q) \bar{\psi}(p_3) \gamma_5 \gamma_\nu \psi(p_2). \quad (60)$$

In Eq. (60) the form of the effective Lagrangian for the  $N^* NA$  vertex is assumed to be the same as that given by Eq. (6).

Analogous expressions can be written for the amplitudes corresponding to the excitation of (spin-1/2 negative parity)  $N^*(1650)$  resonance.

**Pion exchange and  $N^*(1720)$  excitation**

$$M_{N_{3/2}^*}^\pi = - \left( \frac{g_{NN\pi}}{m_\pi} \right) \left( \frac{g_{N_{3/2}^* N \pi}}{m_\pi} \right) \left( \frac{g_{N_{3/2}^* \Lambda K^+}}{m_{K^+}} \right) \bar{\psi}(p_\Lambda) p_{K^+ \delta} G_{N_{3/2}^*}^{\delta\mu}(p) q_\mu \psi(p_1) \\ \times G_\pi(q) \bar{\psi}(p_3) \gamma_5 \gamma_\nu q^\nu \psi(p_2), \quad (61)$$

**$\rho$  meson exchange and  $N^*(1720)$  excitation**

$$M_{N_{3/2}^*}^\rho = -g_{NN\rho} \left( \frac{g_{N_{3/2}^* N \rho}}{m_{N^*} + m_N} \right) \left( \frac{g_{N_{3/2}^* \Lambda K^+}}{m_{K^+}} \right) \bar{\psi}(p_\Lambda) p_{K^+ s} G_{N_{3/2}^*}^{st}(p) (q_\mu g_{t\nu} - q_t g_{\mu\nu}) \gamma^\mu \gamma_5 \psi(p_1) \\ \times G_\rho^{\alpha\nu}(q) \bar{\psi}(p_3) (\gamma_\alpha + \frac{ik_\rho}{2m_N} \sigma_{\alpha\delta} q^\delta) \psi(p_2) \quad (62)$$

**$\omega$  meson exchange and  $N^*(1720)$  excitation**

The form of the amplitude is similar to that of the  $\rho$  meson exchange (Eq. (62)).

**$\sigma$  meson exchange and  $N^*(1720)$  excitation**

$$M_{N_{3/2}^*}^\sigma = -g_{NN\sigma} \left( \frac{g_{N_{3/2}^* N \sigma}}{m_\sigma} \right) \left( \frac{g_{N_{3/2}^* \Lambda K^+}}{m_{K^+}} \right) \bar{\psi}(p_\Lambda) p_{K^+ s} G_{N_{3/2}^*}^{st}(p) q_t \psi(p_1) \\ \times G_\sigma(q) \bar{\psi}(p_3) \psi(p_2) \quad (63)$$

We have not included the contribution of the heavy axial-vector meson into these calculations. Very little is known about the Lagrangian density for its coupling to the spin-3/2 resonance. Moreover, it has been shown earlier [29] that the contribution of these terms to the total meson production cross section is negligible.

The amplitudes given above can be simplified by contracting out the gamma matrices using the Dirac equation whenever applicable. The simplified equations are given in Appendix A. The total amplitude is obtained by summing coherently the amplitudes corresponding to all the processes and graphs.

The general formula for the invariant cross section of the  $p + p \rightarrow p + \Lambda + K^+$  reaction is written as

$$d\sigma = \frac{m_N^3 m_\Lambda}{2\sqrt{[(p_1 \cdot p_2)^2 - m_N^4]}} \frac{1}{(2\pi)^5} \delta^4(P_f - P_i) |A_{fi}|^2 \prod_{a=1}^3 \frac{d^3 p_a}{E_a}, \quad (64)$$

where  $A_{fi}$  represents the total amplitude,  $P_i$  and  $P_f$  the sum of all the momenta in the initial and final states, respectively, and  $p_a$  the momenta of the three particles in the final state. The corresponding cross sections in the laboratory or center of mass systems can be written from this equation by imposing the relevant conditions.

## G. Final state interaction

For describing the data for the  $pp \rightarrow p\Lambda K^+$  reaction at beam energies very close to the threshold, consideration of the final state interaction (FSI) among the three outgoing particles is important. As there exists no theory of the FSI effects in the presence of three

strongly interacting particles, we follow here an approximate scheme in line exactly with Watson-Migdal theory of FSI [44]. In this approach the energy dependence of the cross section due to FSI is separated from that of the primary production amplitude. This method has been applied earlier to study the low momentum behavior of the  $\eta$  meson [45] and pion spectra [46,30,47] measured in proton-proton collisions. We write for the total amplitude

$$A_{fi} = M_{fi}(pp \rightarrow p\Lambda K^+) \cdot T_{ff}, \quad (65)$$

where  $M_{fi}(pp \rightarrow p\Lambda K^+)$  is the primary production amplitude as discussed above, while  $T_{ff}$  describes the re-scattering among the final particles which goes to unity in the limit of no FSI. The latter is taken to be the coherent sum of the two-body on-mass-shell elastic scattering amplitudes of the particles involved in the final channel.

$$T_{ff} = \sum_{i=1}^3 t_i^{\ell_i}(q_i), \quad (66)$$

where  $t_i$  represents the two-body on-shell elastic scattering amplitude (of the interacting particles pair  $j - k$ ) in the three-body space with the  $i$ th particle being the spectator.  $\ell_i$  and  $q_i$  denote the partial wave and relative momentum of the  $j - k$  particle pair.

An assumption inherent in the approximation given by Eq. (65) is that the reaction takes place over a small region of space, a condition fulfilled rather well in near threshold reactions. This allows us to express the amplitudes  $t_i$  in terms of the inverse of the Jost function,  $J_{\ell_i}(q_i)$  [48,30]. In the analysis presented in this paper we assume  $\ell_i = 0$ , for all the three pairs  $j - k$  and use the modified Cini-Fubini-Stanghellini formula [49] for the effective range expansion of the phase-shift ( $\delta_{0i}$ ) of the relevant pair

$$C_0^2 q_i \cot \delta_{0i} + 2q_i \eta h(\eta) = (1/a_i) + (1/2)r_{0i}q_i^2, \quad (67)$$

to calculate the corresponding Jost function. It may be noted that in case of the pair  $j - k$  involving uncharged particle(s), the second terms on the left hand side of Eq. (67) vanishes and  $C_0^2$  goes to unity. In this equation  $r_{0i}$  and  $a_i$  are the effective range and scattering length parameters respectively for the  $j - k$  interacting pair.  $\eta$  is the corresponding Coulomb parameter and

$$C_0^2 = \frac{2\pi\eta}{e^{2\pi\eta} - 1}, \quad h(\eta) = \sum_{n=1}^{\infty} \frac{\eta^2}{n(n^2 + \eta^2)} - 0.5772 - \ln(\eta). \quad (68)$$

In this case we have

$$t_i^0(q_i) = (J_0(q_i))^{-1} = \frac{(q_i^2 + \alpha_i^2)r_{0i}^c/2}{1/a_i^c + (r_{0i}^c/2)q_i^2 - iq_i}, \quad (69)$$

where  $\alpha$  is given by

$$\alpha = (1/r_{0i}^c)[1 + (1 + 2r_{0i}^c/a_i^c)^{1/2}], \quad (70)$$

and  $a_i^c$  and  $r_{0i}^c$  are defined as

$$\frac{1}{a_i^c} = \frac{1}{C_0^2} \left( \frac{1}{a_i} - 2q_i \eta h(\eta) \right) \quad (71)$$

$$r_{0i}^c = \frac{r_{0i}}{C_0^2}. \quad (72)$$

It may be noted that for large  $q_i$ , the amplitude  $t_i$  goes to unity which is to be expected. The extrapolation of the scattering amplitude for the off-shell effects can be achieved by means of a monopole form factor [20]. For a detailed discussion of the off-shell effects we refer to [50].

The factorization of the total amplitude into those of the FSI and primary production (Eq. (65)), enables one to pursue the diagrammatic approach for the latter within an effective Lagrangian model and investigate the role of various meson exchanges and resonances in describing the reaction. Moreover, in this way the FSI among all the three outgoing particles can be included. Although the meson-baryon interactions are weak, they can still be influential through interference.

The parameters  $a$  and  $r_0$  are very poorly known for the  $K^+$ -nucleon and  $K^+$ -hyperon systems as the corresponding scattering data are scarce at low energies. On the other hand, For the hyperon-nucleon system several sets of values for these parameters have been given by the Bonn-Jülich [51] and Nijmegen [52] groups from their respective  $\Lambda - p$  interaction models. There is quite some variation in the values given in these sets. For the  $K^+ - p$  and  $K^+ - \Lambda$  systems we have adopted the values given in a recent effective Lagrangian model analysis of the available  $K\Lambda$  and  $Kp$  data by Feuster and Mosel [53]. In any case, the cross sections are insensitive to the FSI effects in these channels. On the other hand, these effects are very important in  $\Lambda - p$  channel, and we have performed calculation of the corresponding FSI effects with all the sets of these parameters given by Bonn-Jülich and Nijmegen groups (given in Table 3) in order to see if the results are sensitive to various models. More details will be given in the next section.

### III. RESULTS AND DISCUSSION

The theoretical approach presented in the previous section has been used to study the available data on the  $p + p \rightarrow p + \Lambda + K^+$  reaction for beam energies ranging from just above the production threshold to about 10 GeV. In the results shown below, we have used PS couplings for both  $N^*N\pi$  and  $N^*\Lambda K^+$  vertices involving spin-1/2 resonances of even and odd parities. However, calculations have also been performed with the corresponding PV couplings. The cross sections calculated with this option for the resonance-hyperon-kaon vertex deviates very little from those obtained with the corresponding PS couplings. However, the PV coupling for the  $N^*N\pi$  vertex leads to noticeably different results as is discussed below.

#### A. Cross section data for beam energy above 2 GeV

In Fig. 2 we show the comparison of our calculations with the experimental data for the total cross section for this reaction as a function of beam momentum for incident energies

above 2 GeV. In this figure we have investigated the role of various meson exchange processes to the total cross section. The dotted, dashed, long-dashed and dashed-dotted curves represent the contributions of  $\pi$ ,  $\rho$ ,  $\omega$  and  $\sigma$  meson exchanges respectively. The contribution of the heavy axial meson exchange is not shown in this figure as they are negligibly small. The coherent sum of all the meson-exchange processes is shown by the solid line. The experimental points are taken from [15]. We notice that the measured cross sections are reproduced reasonably well by our calculations (solid line) for all the beam energies except for two lowest points. The FSI effects which are not included in these calculations, reduce the discrepancy between the experimental data and calculations at these beam momenta. This point is discussed in the next subsection.

We note that the pion exchange graphs dominate the production process for all the energies. In comparison to this, the contributions of  $\rho$  and  $\omega$  meson exchanges are almost insignificant. The  $\rho$ -meson exchange, which is a convenient way of taking into account the  $P$  wave part of the correlated two-pion exchange (CTPE) process, is rather weak even in the low energy  $NN$  scattering [41]. With increasing projectile energy its contribution decreases further. On the other hand, the  $\sigma$  meson exchange, which models the CTPE in the  $\pi\pi$  S-wave and provides about 2/3 of this exchange in the low energy  $NN$  interaction, plays a relatively more important role. This observation has also been made in the case of  $NN \rightarrow NN\pi$  reaction [54-56,29,30]. Thus, the  $\sigma$  meson exchange provides an efficient means of mediating the large momentum mismatch involved in the meson production reactions in  $NN$  collisions, particularly at lower beam momenta.

The relative importance of the contributions of each intermediate resonance to the  $pp \rightarrow p\Lambda K^+$  reaction is studied in Fig. 3, where the decomposition of the contributions from  $N^*(1710)$ ,  $N^*(1720)$  and  $N^*(1650)$  resonances to the energy dependence of the total cross section are shown by dotted, dashed and dashed-dotted lines respectively. Their coherent sum is depicted by the solid line. It is clear that the contributions from the  $N^*(1710)$  and  $N^*(1650)$  resonances dominate the total cross section at beam momenta above and below 3 GeV/c respectively. Moreover, the interference terms of the amplitudes corresponding to various resonances are quite important. This result is in sharp contrast to the resonance model calculations of Refs. [21,22,24], where these terms were ignored conjecturing them to be negligible.

Looking in Table 2, one might naively expect the dominance of the  $N^*(1710)$  resonance everywhere as the coupling constants for the  $N^*\Lambda K^+$  and  $N^*N\pi$  vertices for the  $N^*(1710)$  resonance are about an order of magnitude larger than those for  $N^*(1720)$  and  $N^*(1650)$  resonances. In fact, the relative importance of various resonances is determined by the dynamics of the reaction mechanism. As the beam energy rises above the  $K^+$  production threshold, the excitation of the resonance lowest in energy is more probable in the beginning. With the increasing beam energy the excitation of the higher energy resonances starts playing more and more important role.

As mentioned earlier, the use of the PV coupling for the  $N^*\Lambda K$  vertices (involving spin-1/2 even and odd parity resonances) makes insignificant changes in the cross sections. However, there is a clear preference for the PS coupling at the  $N^*N\pi$  vertices. This is shown in Fig. 4, where the ratio of the total cross section obtained by using the PV ( $\sigma_{PV}$ ) and PS ( $\sigma_{PS}$ ) couplings for these vertices, is shown as a function of the beam momentum. It is seen that  $\sigma_{PV}$  is larger than  $\sigma_{PS}$  at higher beam momenta while at lower ones the reverse is true.

Clearly PS coupling for the  $N^*N\pi$  vertex provides a better description of the beam energy dependence of the total cross section for the  $pp \rightarrow pK^+\Lambda$  reaction.

## B. Cross section data for beam energies below 2 GeV

In Fig. 5 we compare the results of our calculations (with FSI effects included) with the recent data [16] for the  $pp \rightarrow pK^+\Lambda$  reactions at beam energies very close to the kaon production threshold. In this figure the total cross section is shown as a function of the excess energy ( $\epsilon$ ) =  $\sqrt{s} - m_N - m_{K^+} - m_\Lambda$ , where  $\sqrt{s}$  is the invariant mass. The FSI effects were included by following the procedure outlined in section 2.G. We have chosen [53]  $a = 0.065 + i0.040$ ,  $r_0 = -15.930 - i8.252$  and  $a = -0.214$ ,  $r_0 = -0.331$  for the  $K^+\Lambda$  and  $K^+p$  systems respectively in all the calculations shown below. For the  $\Lambda - p$  system all the seven sets of the parameters as shown in Table 3 were used.

In Fig. 5a, the results obtained with the parameters sets of models A (solid line),  $\tilde{A}$  (dotted line), B (dashed line) and  $\tilde{B}$  (dashed-dotted line) of the Bonn-Jülich group [51] are shown. It can be noted that all the four models provide similar results for the total cross sections at  $\epsilon \sim 150$  MeV. However, at lower values of  $\epsilon$ , cross section calculated with models A, and  $\tilde{A}$  are larger than those of model B and  $\tilde{B}$  by a factor of about 2-3. Moreover, there is a difference of a factor of more than 2 between the results obtained with model A and  $\tilde{A}$  itself; the former provides a better agreement with the data. The results obtained with the models D, E and NSC of the Nijmegen group [52] are shown in Fig. 5b. These three models produce almost identical results for all the values of  $\epsilon$ . However, while the data at the higher excess energies are reproduced by all the three model quite well, they under-predict the cross sections at lower  $\epsilon$  by a factor of about 3. Therefore, while all the models of  $\Lambda - p$  interactions provide an equally good description of the total cross section data at higher values of the excess energy, a difference of factors of 2-3 occurs between their predictions at lower values. Thus, the near threshold  $\Lambda K^+$  production data in proton-proton collisions are sensitive to the S-wave  $\Lambda$ -nucleon interaction and may be used to distinguish between various models proposed in the literature to describe this interaction. We note that model A of the Bonn-Jülich group provides the best overall description of the data, which has been used to account for the  $\Lambda - p$  FSI effects in all the calculations discussed subsequently.

The individual contributions of various nucleon resonances to the total cross section of the  $pp \rightarrow p\Lambda K^+$  reaction near the production threshold is shown in Fig. 6, as a function of the excess energy. In contrast to the situation at higher beam energies ( $p_{lab} \geq 3$  GeV/c), the cross section is dominated by the  $N^*(1650)$  resonance excitation. This is in line with the observations made in Ref. [23]. Since this is the lowest energy baryonic resonance having an appreciable branching ratio for the decay to the  $\Lambda K^+$  channel, its dominance in this reaction at beam energies near the kaon production threshold is to be expected. The contributions of other two resonances ( $N^*(1710)$  and  $N^*(1720)$ ) are several orders of magnitude smaller, therefore, the resonance-resonance interference terms are also very small. Thus, near threshold energies, this reaction proceeds preferentially via excitation of the  $N^*(1650)$  resonance. This conclusion is in contrast with the results reported in Ref [24] where it is claimed that the low energy data do not provide a clear clue about the nature of resonance excitation. This is based on the results of the calculations performed by these authors (within the resonance model) of the invariant mass spectrum of the  $\Lambda K^+$  pair, whose



shape remain similar to that of the pure phase space even after considering the excitation  $N^*(1650)$  resonance. However, the FSI effects have not been included in these calculations. These effects which depend on the relative energy of the out-going particle pairs (and hence on the excitation of the particular resonances) may change their invariant mass spectrum at near threshold beam energies. Furthermore, it is not clear if these authors have used energy dependent widths in the denominators of the resonance propagators (see Eqs.(54)-(56)). This is also expected to influence the invariant mass spectrum of the outgoing particle pairs.

In Fig. 7, we show the contributions of various meson exchanges to this reaction at near threshold beam energies. Various curves have the same meaning as in Fig. 2. The one pion exchange graphs dominate the reaction in this energy regime as well. On the other hand, the individual contributions of the  $\rho$  and  $\omega$  meson exchange processes are negligible. However, that of the  $\sigma$  meson exchange is substantial in this energy regime. Thus, like near threshold pion production in proton-proton collisions, the heavy scalar meson exchange plays an important role in this case too. It should however, be noted that the interference terms of various meson exchange processes are not negligible; contributions of various exchange processes simply do not add up to the total cross section obtained by the coherent addition of various amplitudes.

#### IV. SUMMARY AND CONCLUSIONS

We investigated the associated  $K^+\Lambda$  production in the proton-proton collisions at energies ranging from near threshold to about 10 GeV. This reaction is of interest as it provides the prospect of testing QCD in the non-perturbative domain at energies larger than the pion mass. In this paper our goal has been to investigate this reaction within an effective Lagrangian model which is proven to be very successful in describing the pion production in  $NN$  collisions. Most of the parameters of this model are fixed by fitting to the elastic  $NN$  T-matrix; this restricts the freedom of varying the parameters of the model to provide a fit to the data. The reaction proceeds via the excitation of the  $N^*(1650)$ ,  $N^*(1710)$  and  $N^*(1720)$  intermediate nucleon resonant states. The coupling constants at vertices involving resonances have been determined from the experimental branching ratios of their decay into various relevant channels. Unlike the  $NN\pi$  vertex, there is no compelling reason to choose the pseudovector (PV) form for the  $N^*\Lambda K^+$  and  $N^*N\pi$  couplings (involving spin-1/2 resonances of even and odd parities) and we investigated both the PV and pseudoscalar (PS) couplings at these vertices. To describe the data at the near threshold beam energies, we have included the FSI effects among the outgoing particles by following Watson-Migdal theory which has been used before successfully to describe the  $NN\eta$  and  $NN\pi$  reactions in the similar energy regimes.

With the same set of parameters, the model is able to provide a good description of the data at higher as well as near threshold beam energies. The one pion exchange processes make the dominant contribution to the cross section in the entire energy regime. The individual contributions of the  $\rho$  and  $\omega$  meson exchange diagrams is very small every where. Although, the interference terms of their amplitudes with those of other meson exchanges may still be noticeable. On the other hand, the  $\sigma$  exchange makes a relatively larger contribution at lower beam energies, confirming the earlier observation that the heavy scalar meson provides a means of mediating the large momentum transfer in near threshold  $NN$ -meson

production processes.

While at beam momenta larger than 3 GeV/c, the reaction proceeds predominantly via excitation of the  $N^*(1710)$  resonance, the process gets maximum contribution from the  $N^*(1650)$  resonance at lower beam energies. A very striking feature of our results is that the interference among various resonance contributions is very significant. Therefore, the conjecture made in previous studies of this reaction that these terms are negligible must be viewed with caution. The near threshold data clearly favors the excitation of the  $N^*(1650)$  resonance. Therefore, this reaction, in this energy regime, provides an ideal means of investigating the properties of this baryonic resonance.

Unlike the  $NN\pi$  vertex where there is a clear preference for the PV coupling, as seen in the  $NN\pi$  data, the present reaction does not distinguish between PS and PV couplings at the  $N^*\Lambda K^+$  vertex involving spin-1/2 even or odd parity resonance. However, the PS coupling at the  $N^*N\pi$  vertex is clearly favored by data.

The near threshold data may be selective about the model describing the low energy  $\Lambda$ -nucleon scattering. Calculations of the FSI effects performed with the scattering length and effective range parameters of the Jülich-Bonn group produce different results as compared to those performed with the corresponding parameters of the Nijmegen group. The parameters of model A of Ref. [51] provides the best agreement with data.

An obvious extension of the present work is to calculate the cross sections for the  $pp \rightarrow p\Sigma K^+$  reaction. There is a proposal to measure this reaction at COSY in Jülich. This will also lead to the inclusive  $K^+$  cross sections in the elementary nucleon-nucleon collisions which are the necessary input to the transport model calculations of the strangeness production in the heavy ion collisions. This work is currently underway by extending the model to include the excitation of nucleon resonances  $N^*(1990)$  and delta isobars  $\Delta(1910)$  and  $\Delta(1920)$  which are four star and three star resonances respectively.

## ACKNOWLEDGMENTS

The authors is thankful to Ulrich Mosel for his very kind hospitality during several visits to the University of Giessen and for numerous useful discussions which were very helpful in completing this work. He is also thankful to Wolfgang Nörenberg and Jörn Knoll for their warm hospitality in the theory group of the GSI where this work was initiated. Useful discussions with W. Cassing, B. Friman, G. Penner, W. Peters, M. Post and A. Sibirtsev are gratefully acknowledged. The author is thankful to the Abdus Salam International Center for Theoretical Physics, Trieste for providing him an associateship award.

## APPENDIX A:

By using the straightforward algebra of  $\gamma$  matrices and the Dirac equation the amplitudes given in section 2.F can be rewritten in the forms which are suitable for numerical calculations.

*Pion exchange and  $N^*(1710)$  excitation*

$$M_{N_{1/2}^*}^\pi = -g_{NN\pi} g_{N_{1/2}^* \Lambda K^+} \frac{g_{N_{1/2}^* N \pi}}{m_{N^*} + m_N} \frac{1}{q^2 - m_\pi^2} \frac{1}{p^2 - (m_{N^*} - i\Gamma_{N_{1/2}})^2} \bar{\psi}(p_3) \gamma_5 \psi(p_2) \times \bar{\psi}(p_\Lambda) (A + B) \psi(p_1) \quad (\text{A1})$$

where with the PV coupling for the  $N^* N \pi$  vertex the constants A and B are given by,

$$A = -p^2 + m_\Lambda m_N + (m_\Lambda - m_N) m_{N^*}, \quad (\text{A2})$$

$$B = m_{N^*} + m_N. \quad (\text{A3})$$

With the corresponding PS coupling these constants are

$$A = (m_{N^*} + m_N)(m_{N^*} - m_\Lambda), \quad (\text{A4})$$

$$B = -(m_{N^*} + m_N). \quad (\text{A5})$$

*$\rho$  meson exchange and  $N^*(1710)$  excitation*

$$M_{N_{1/2}^*}^\rho = g_{NN\rho} g_{N_{1/2}^* \Lambda K^+} g_{N_{1/2}^* N \rho} \frac{1}{q^2 - m_\rho^2} \frac{1}{p^2 - (m_{N^*} - i\Gamma_{N_{1/2}})^2} \bar{\psi}(p_\Lambda) C \psi(p_1), \quad (\text{A6})$$

where C is defined as

$$C = \frac{1}{4m_N} [m_\Lambda \gamma_\beta q^\beta \gamma_\alpha b^\alpha \gamma_5 + \gamma_\eta p_K^\eta \gamma_\beta q^\beta \gamma_\alpha b^\alpha \gamma_5 - m_{N^*} \gamma_\beta q^\beta \gamma_\alpha b^\alpha \gamma_5 - m_\Lambda \gamma_\alpha b^\alpha \gamma_\beta q^\beta \gamma_5 - \gamma_\eta p_K^\eta \gamma_\alpha b^\alpha \gamma_\beta q^\beta \gamma_5 + m_{N^*} \gamma_\alpha b^\alpha \gamma_\beta q^\beta \gamma_5], \quad (\text{A7})$$

with

$$b^\mu = \bar{\psi}(p_3) [(1 + k_\rho) \gamma^\mu + \frac{k_\rho}{m_N} (-p_3^\mu - (p_3 q / q^2) q^\mu)] \psi(p_2). \quad (\text{A8})$$

*$\sigma$  exchange and  $N^*(1710)$  excitation*

$$M_{N_{1/2}^*}^\sigma = -g_{NN\sigma} g_{N_{1/2}^* \Lambda K^+} g_{N_{1/2}^* N \sigma} \frac{1}{q^2 - m_\sigma^2} \frac{1}{p^2 - (m_{N^*} - i\Gamma_{N_{1/2}})^2} \bar{\psi}(p_3) \psi(p_2) \times \bar{\psi}(p_\Lambda) [(m_{N^*} - m_\Lambda) \gamma_5 - \gamma_\mu p_K^\mu \gamma_5] \psi(p_1) \quad (\text{A9})$$

*Pion exchange and  $N^*(1720)$  excitation*

$$M_{N_{3/2}^*}^\pi = - \left( \frac{g_{NN\pi}}{m_\pi} \right) \left( \frac{g_{N_{3/2}^* N \pi}}{m_\pi} \right) \left( \frac{g_{N_{3/2}^* \Lambda K^+}}{m_{K^+}} \right) \frac{1}{q^2 - m_\pi^2} \frac{1}{p^2 - (m_{N_{3/2}^*} - i\Gamma_{N_{3/2}})^2} \bar{\psi}(p_3) \gamma_5 \psi(p_2) \bar{\psi}(p_\Lambda) (C + D \gamma_\mu p_K^\mu) \psi(p_1) \quad (\text{A10})$$

where

$$\begin{aligned}
C = & m_\Lambda p_K q - \frac{2}{3} m_\Lambda p_K p + \frac{1}{3} m_\Lambda m_K^2 + \frac{1}{3} (m_\Lambda - m_N) p_K p + m_{N^*} p_K q - \frac{2}{3} m_{N^*} p_K p \\
& + \frac{1}{3} m_{N^*} m_K^2 - \frac{1}{3} (m_\Lambda - m_N) m_K^2 - \frac{2(p_K p)(p q)}{3m_{N^*}^2} m_\Lambda - \frac{(p_K p)m_K^2}{3m_{N^*}} - \frac{(p q)m_K^2}{3m_{N^*}} \\
& + \frac{2(p_K p)^2}{3m_{N^*}} + \frac{(p_K p)(m_\Lambda^2 - m_N m_\Lambda)}{3m_{N^*}} - \frac{2(p_K p)(p q)}{3m_{N^*}} \tag{A11}
\end{aligned}$$

$$\begin{aligned}
D = & p_K q + \frac{1}{3} m_\Lambda (m_\Lambda + m_N) - \frac{1}{3} m_K^2 + \frac{1}{3} m_{N^*} (m_N + m_\Lambda) + \frac{1}{3} p_K p - \frac{1}{3} p q \\
& - \frac{2(p_K p)(p q)}{3m_{N^*}^2} - \frac{(p_K p)m_N}{3m_{N^*}} - \frac{(p q)m_\Lambda}{3m_{N^*}} \tag{A12}
\end{aligned}$$

$\rho$  exchange and  $N^*(1720)$  excitation

$$\begin{aligned}
M_{N_{3/2}^*}^\rho = & -g_{NN\rho} \left( \frac{g_{N_{3/2}^* N \rho}}{m_{N^*} + m_N} \right) \left( \frac{g_{N_{3/2}^* \Lambda K^+}}{m_{K^+}} \right) \frac{1}{q^2 - m_\rho^2} \\
& \bar{\psi}(p_\Lambda) [p_{Ks} G_{N_{3/2}^*}^{s\nu} q^\lambda \gamma_\lambda \gamma_5 - p_{Ks} G^{st} q_t \gamma^\nu \gamma_5] \psi(p_1) \bar{\psi}(p_3) [(1 + k_\rho) \gamma_\nu - \frac{k_\rho}{m_N} p_{3\nu}] \psi(p_2), \tag{A13}
\end{aligned}$$

This equation can be further simplified by using the form of the propagator  $G_{N_{3/2}^*}^{st}$  (Eq. (53)). These expressions are not being given here as they are very lengthy even though it is straightforward to derive them.

$\sigma$  exchange and  $N^*(1720)$  excitation

$$\begin{aligned}
M_{N_{3/2}^*}^\sigma = & -g_{NN\sigma} \left( \frac{g_{N_{3/2}^* N \sigma}}{m_\sigma} \right) \left( \frac{g_{N_{3/2}^* \Lambda K^+}}{m_{K^+}} \right) \frac{1}{q^2 - m_\sigma^2} \frac{1}{p^2 - (m_{N_{3/2}^*} - i\Gamma_{N_{3/2}})^2} \\
& \bar{\psi}(p_3) \psi(p_2) \bar{\psi}(p_\Lambda) (E + F \gamma_\mu p_K^\mu) \psi(p_1) \tag{A14}
\end{aligned}$$

where E and F are the same as C and D respectively.,

The numerical evaluation of the amplitudes can be carried out very conveniently by using the techniques of the Clifford algebra.

## REFERENCES

- [1] T.E.O Ericson and W. Weise, *Pions and Nuclei*, Clarendon, Oxford, 1988.
- [2] M. Alberg, Prog. Part. Nucl. Phys. **36**, 217 (1996).
- [3] A. Deloff, Nucl. Phys.A **505**, 583 (1989)
- [4] R.A. Adelseck and B. Saghai, Phys. Rev.C **42**, 108 (1990).
- [5] U. Mosel, Ann. Rev. Nucl. Part. Sci. **41**, 29 (1991) and references therein.
- [6] G.E. Brown, C.M. Ko, Z.G. Wu and L.H. Xia, Phys. Rev.C **43**, 1881 (1991).
- [7] T. Maruyama, W. Cassing, U.Mosel, S. Teis and K. Weber, Nucl. Phys.A **573**, 653 (1994).
- [8] D. Miskowiec et al., Phys. Rev. Lett. **72**, 3650 (1994).
- [9] C. Hartnack, J. Jaenicke, L. Sehn, H. Ströcker and J. Aichelin, Nucl. Phys.A **580**, 643 (1994).
- [10] X.S. Fang, C.M. Ko, G.Q. Li, Y.M. Zheng, Nucl. Phys.A **575**, 766 (1994).
- [11] G.Q. Li and C.M. Ko, Phys. Lett.B **349**, 405 (1995).
- [12] G.Q. Li, C.M. Ko and W.S. Chung, Phys. Rev.C **57**, 434 (1998).
- [13] J. Rafelski and B. Müller, Phys. Rev. Lett. **48**, 1066 (1982).
- [14] H.W. Barz, B.L. Friman, J. Knoll and H. Schulz, Nucl. Phys.A **485**, 685 (1988).
- [15] Landolt-Börnstein, New Series, Ed. H. Schopper, I/12 (1988).
- [16] J.T. Balewski et al., Phys. Lett. B **388**, 859 (1996); Phys. Lett. B **420**, 211 (1998); R. Bilger et al., Phys. Lett.B **420**, 217 (1998).
- [17] E. Ferrari, Nuovo cimento **15**, 652 (1960); E.Ferrari, Phys. Rev. **120**, 988 (1960).
- [18] T. Yao, Phys. Rev. **125**, 1048 (1962).
- [19] J.Q. Wu and C.M. Ko, Nucl. Phys.A **499**, 810 (1989).
- [20] J.M. Laget, Phys. Lett.B **259**, 24 (1991).
- [21] K. Tsushima, S.W. Huang and Amand Faessler, Phys. Lett.B **337**, 245 (1994).
- [22] K. Tsushima, A. Sibirtsev and A.W. Thomas, Phys. Lett.B **390**, 29 (1997).
- [23] G. Fäldt and C. Wilkin, Z. Phys.A **357**, 241 (1997).
- [24] A. Sibirtsev, K. Tsushima and A.W. Thomas, Phys. Lett.B **421**, 59 (1998).i
- [25] S. Weinberg, Phys. Rev. **166**, 1568 (1968).
- [26] R.D. Peccei, Phys. Rev. **181**, 1902 (1969).
- [27] R.M. Davidson, N.C. Mukhopadhyay, and R.S. Wittman, Phys. Rev.D **43**, 71 (1991).
- [28] M. Benmerrouche, N.C. Mukhopadhyay, and J.F. Zhang, Phys. Rev.D **51**, 3237 (1995).
- [29] A. Engel, R. Shyam, U. Mosel and A.K. Dutt-Majumdaer, Nucl. Phys.A **603**, 387 (1996).
- [30] R. Shyam and U. Mosel, Phys. Lett.B **426**, 1 (1998).
- [31] J.D. Bjorken and S.D. Drell, *Relativistic Quantum Mechanics*, McGraw-Hill, New York, 1964.
- [32] M. Schäfer, H.C. Dönges, A. Engel and U. Mosel, Nucl. Phys.A **575**, 429 (1994).
- [33] N. Dombay and B.J. Read, Nucl. Phys.B **60**, 65 1973.
- [34] Particle Data Group, C. Casso et al, Eur. Ohys. J. C **3**, 1 (1998).
- [35] T. Feuster and U. Mosel, Nucl. Phys.A **612**, 375 (1997).
- [36] M. Benmerrouche, R.M. Davidson and N.C. Mukhopadhyay, Phys. Rev.C **39**, 2339 (1989).
- [37] B. Friman and H.J. Pirner, Nucl. Phys.A **617**, 496 (1997)
- [38] R. Rapp, G. Chanfray and J. Wambach, Nucl. Phys.A **617**, 472 (1997).

- [39] W. Peters, M. Post, H. Lenske, S. Leupold and U. Mosel, Nucl. Phys.A **632**, 109 (1998).
- [40] J.J. Sakurai, *Currents and Mesons*, Univ. of Chicago Press, Chicago, 1969; Ann. Phys. **11**, 1 (1960).
- [41] R. Machleidt, K. Hollinde and Ch. Elster, Phys. Rep. **149**, 1 (1987).
- [42] A. König and P. Kroll, Nucl. Phys.A **356**, 345 (1981).
- [43] C. Itzykson and J.B. Zuber, *Quantum Field Theory*, McGraw-Hill, New York, 1964.
- [44] K.M. Watson, Phys. Rev. **88**, 1163 (1952); A.B. Migdal, Soviet Phys. JETP **1**, 2 (1955).
- [45] A. Moalem, E. Gedalin, L. Razdolskaja, Z. Shorer, Nucl. Phys.A **589**, 649 (1995), Nucl. Phys.A **600**, 445 (1996).
- [46] J. Dubach, W.M. Kloet, R.R. Silbar, Phys. Rev.C **33**, 373 (1986).
- [47] V. Bernard, N. Kaiser and Ulf-G. Meissner, LANL preprint nucl-th/9806013.
- [48] M.L. Goldberger and K.M. Watson, *Collision Theory*, Wiley, New York, 1969, pp. 549.
- [49] H.P. Noyes, Ann. Rev. Nucl. Sci. **22**, 465 (1972).
- [50] C. Hanhart and K. Nakayama, LANL preprint, nucl-th/9809059.
- [51] A. Reuber, K. Hollinde and J. Speth, Nucl. Phys.A **570**, 543 (1994).
- [52] P.M.M. Maessen, T.A. Rijken and J.J. de Swart, Phys. Rev.C **40**, 2226 (1989).
- [53] T. Feuster and U. Mosel, Phys. Rev.C **58**, 457 (1998); T. Feuster, (private communication).
- [54] V. Dmitriev, O. Sushkov and C. Gaarde, Nucl. Phys.A **459**, 503 (1986).
- [55] T.S.H. Lee and D.O. Riska, Phys.Rev.Lett, Phys. Rev. Lett. **70**, 1137 (1993).
- [56] C.J. Horowitz, H.O. Meyer and D.K. Griger, Phys. Rev.C **49**, 1337 (1994).

TABLES

TABLE I. Coupling constants for the  $NN$ -meson vertices used in the calculations

Meson	$g^2/4\pi$	$\ell$	$\Lambda$ (GeV)	mass (GeV)
$\pi$	12.562	0.1133	1.005	0.138
$\sigma$	2.340	0.1070	1.952	0.550
$\omega$	46.035	0.0985	0.984	0.783
$\rho$	0.317	0.1800	1.607	0.770

$k_\rho = 6.033, k_\omega = 0.0, g_{\rho\pi\pi} = 2g_\rho$

TABLE II. Coupling constants and cut-off parameters for the  $N^*N$ -meson and  $N^*$ -hyperon-meson vertices used in the calculations

Resonance	Width (GeV)	Decay channel	Adopted value of the branching ratio	$g^2/4\pi$	cut-off (GeV)
$N^*(1710)$	100	$N\pi$	0.150	0.0863	850.0
		$N\rho$	0.150	1.3653	850.0
		$N\omega$		0.1189	850.0
		$N\sigma$	0.650	0.1381	850.0
		$\Lambda K$	0.150	2.9761	850.0
$N^*(1720)$	150	$N\pi$	0.150	0.0034	850.0
		$N\rho$	0.775	100.10	850.0
		$N\omega$		22.810	850.0
		$N\sigma$	0.770	0.3392	850.0
		$\Lambda K$	0.065	0.0594	850.0
$N^*(1650)$	150	$N\pi$	0.700	0.0521	850.0
		$N\rho$	0.150	0.6806	850.0
		$N\omega$		0.2582	850.0
		$N\sigma$	0.150	1.7290	850.0
		$\Lambda K$	0.070	0.0485	850.0



TABLE III. Scattering length ( $a$ ) and effective range ( $r_0$ ) parameters for the  $\Lambda N$  scattering derived from models A,  $\tilde{A}$ , B and  $\tilde{B}$  of the Jülich-Bonn group [51] and D, F and NSC of the Nijmegen group [52].

model	$a(\text{singlet})$ (fm)	$r_0(\text{singlet})$ (fm)	$a(\text{triplet})$ (fm)	$r_0(\text{triplet})$ (fm)
A	1.56	1.43	1.59	3.16
$\tilde{A}$	2.04	0.64	1.33	3.91
B	0.56	7.77	1.91	2.43
$\tilde{B}$	0.40	12.28	2.12	2.57
D	1.90	3.72	1.96	3.24
F	2.29	3.17	1.88	3.36
NSC	2.78	2.88	1.41	3.11

## Figure Captions

- Fig. 1 Feynman diagrams for  $K^+\Lambda$  production in  $pp$  collisions. The diagram on the left shows the direct process while that on the right the exchange one.
- Fig. 2 The total cross section for the  $p + p \rightarrow p + K^+ + \Lambda$  reaction as a function of the beam momentum. The dotted, dashed, long-dashed and dashed-dotted curves represent the contributions of  $\pi$ ,  $\rho$ ,  $\omega$  and  $\sigma$  meson exchanges respectively. Their coherent sum is shown by the solid line. The experimental data are from [15].
- Fig. 3 Contributions of  $N^*(1710)$  (dotted line),  $N^*(1720)$  (dashed-dotted line) and  $N^*(1650)$  (dashed line) baryonic resonances to the total cross section for the  $p + p \rightarrow p + K^+ + \Lambda$  reaction as a function of beam momentum. Their coherent sum is shown by the solid line.
- Fig. 4 Ratio of the total cross section calculated with pseudovector and pseudoscalar couplings for the  $N^*N\pi$  vertex for spin-1/2 (even and odd parity) resonance for the same reaction as in Fig. 2, as a function of beam momentum.
- Fig. 5 The total cross section for the  $p + p \rightarrow p + K^+ + \Lambda$  reaction very close to the  $K^+$  production threshold as a function of the excess energy (defined in the text). The FSI effects are included by using the scattering length ( $a$ ) and effective range ( $r_0$ ) parameters for the  $K^+ - \Lambda$  and  $K^+ - p$  systems taken from the Ref. [53] and those for the  $\Lambda - p$  system from the sets given by Jülich-Bonn [51] and Nijmegen [52] groups. In the upper part (a) results obtained with the  $\Lambda - p$  parameters of models A (solid line),  $\tilde{A}$  (dotted line), B (dashed line) and  $\tilde{B}$  (dashed-dotted line) of the former group are shown, while in the lower part (b) those of models D, F and NSC of the latter group are depicted. The results of the three models of the Nijmegen group are indistinguishable from each other. The experimental data are taken from [15,16].
- Fig. 6 Contributions of  $N^*(1710)$  (dotted line),  $N^*(1720)$  (dashed-dotted line) and  $N^*(1650)$  (dashed line) baryonic resonances to the total cross section for the same reaction as in Fig. 5, as a function of the excess energy. Their coherent sum is shown by the solid line. The FSI effects are included with  $a$  and  $r_0$  parameters of the  $K^+ - p$  and  $K^+ - \Lambda$  systems being the same as those in Fig. 5 and those for the  $\Lambda - p$  system being taken from model A of the Jülich-Bonn group citeholl94. The experimental data are from [16,15].
- Fig. 7 Contributions of  $\pi$  (dotted line),  $\rho$  (dashed line),  $\omega$  (long-dashed line) and  $\sigma$  (dashed-dotted line) meson exchange processes to the total cross section for the same reaction as shown in Fig. 6, as a function of the excess energy. Their coherent sum is shown by the solid line. The FSI effects are included in the same way as in Fig. 6. The experimental data are from [16,15].

FIGURES

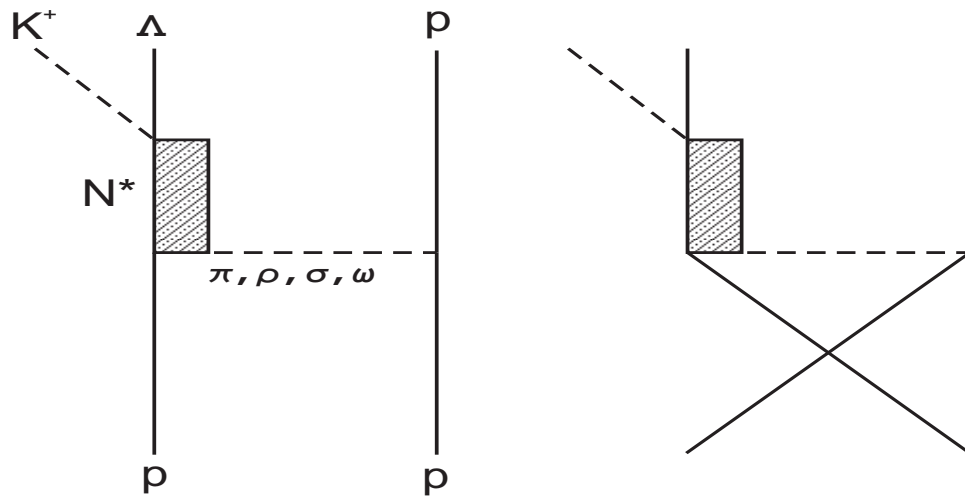


FIG. 1. Feynman diagrams for  $K^+\Lambda$  production in  $pp$  collisions. The diagram on the left shows the direct process while that on the right the exchange one.

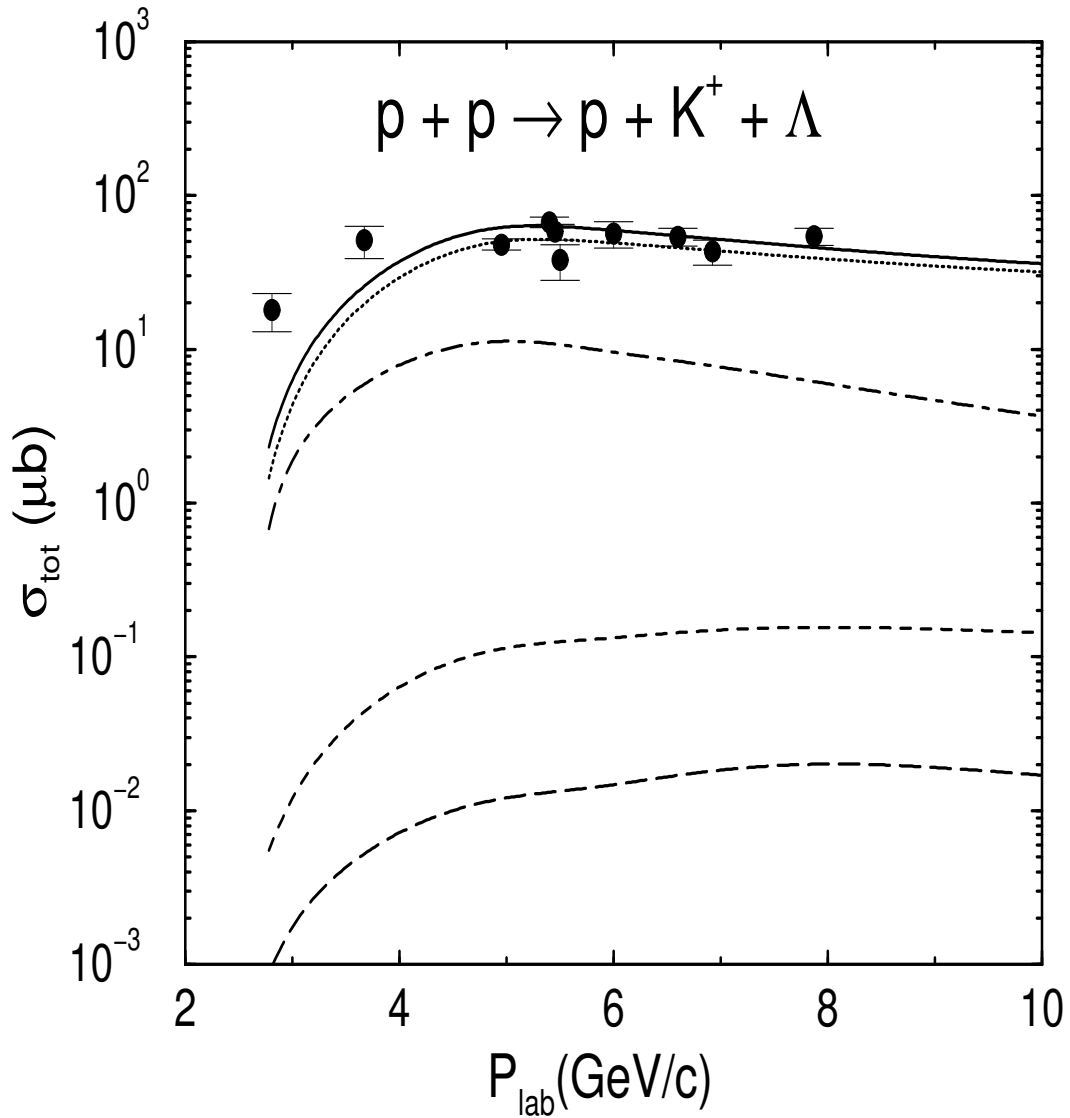


FIG. 2. The total cross section for the  $p + p \rightarrow p + K^+ + \Lambda$  reaction as a function of the beam momentum. The dotted, dashed, long-dashed and dashed-dotted curves represent the contributions of  $\pi$ ,  $\rho$ ,  $\omega$  and  $\sigma$  meson exchanges respectively. Their coherent sum is shown by the solid line. The experimental data are from the Ref. [15].

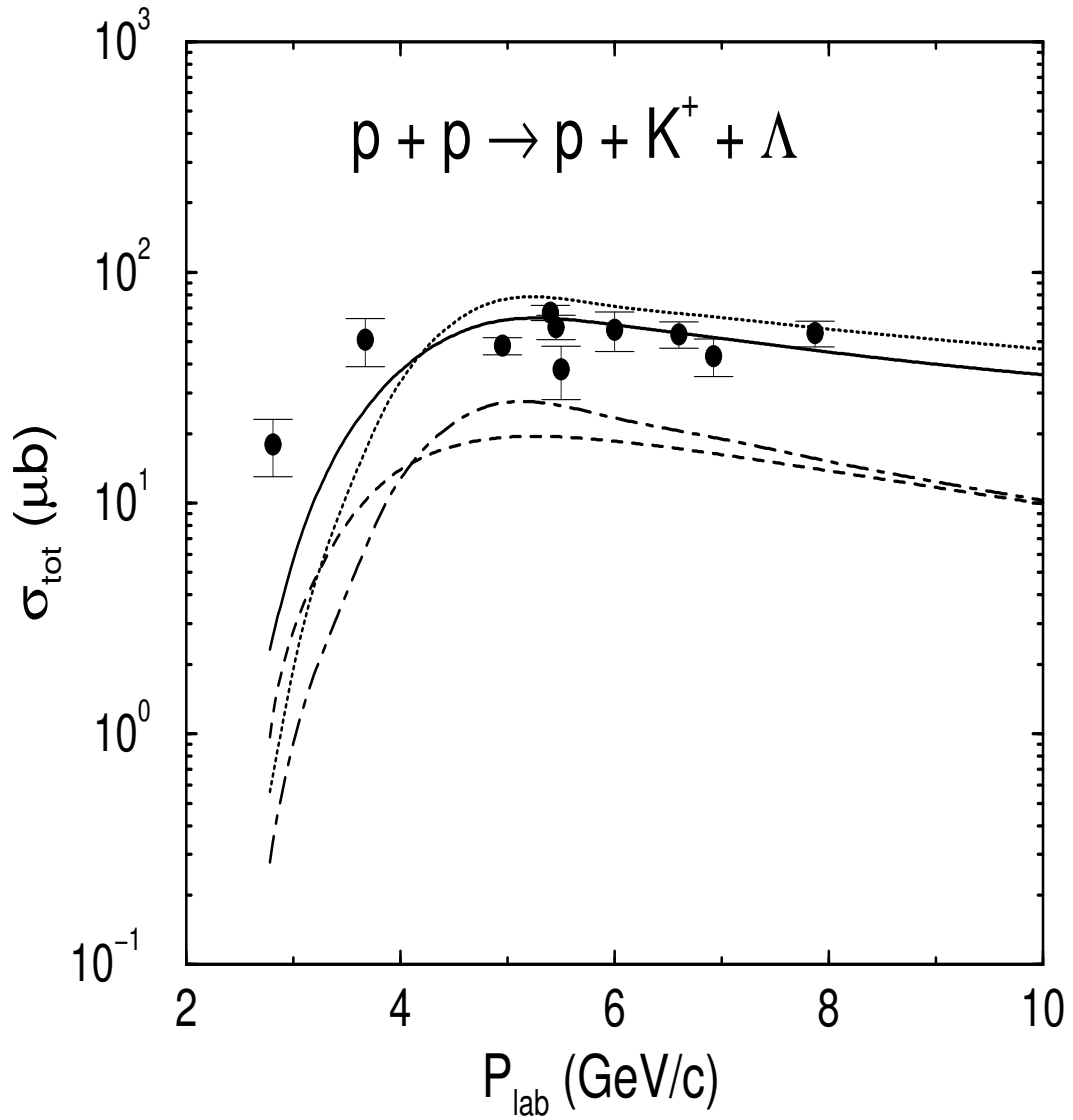


FIG. 3. Contributions of  $N^*(1710)$  (dotted line),  $N^*(1720)$  (dashed-dotted line) and  $N^*(1650)$  (dashed line) baryonic resonances to the total cross section for the  $pp \rightarrow p + K^+ + \Lambda$  reaction as a function of beam momentum. Their coherent sum is shown by the solid line.

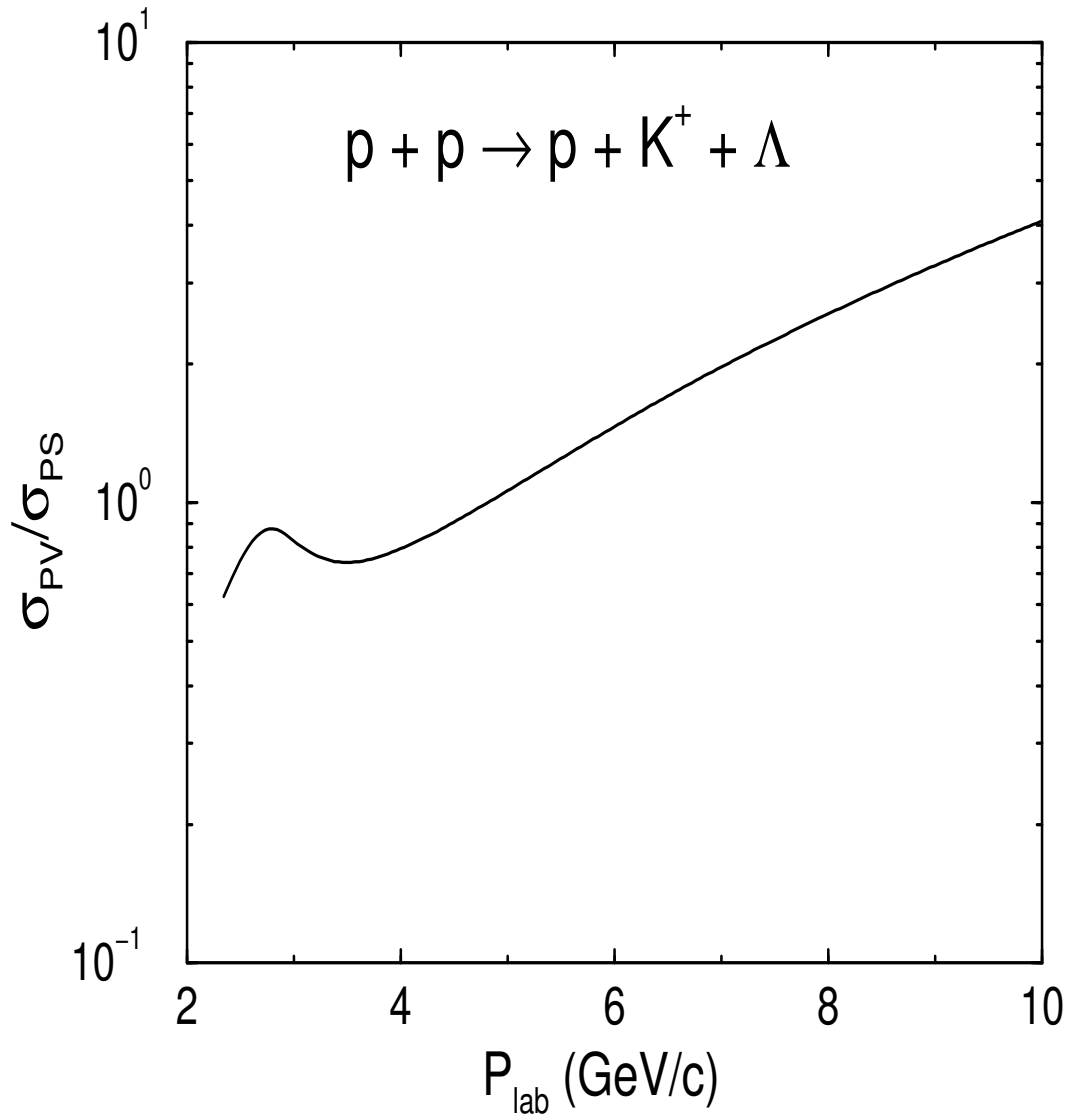


FIG. 4. Ratio of the total cross section calculated with pseudovector and pseudoscalar couplings for the  $N^*N\pi$  vertex corresponding to spin-1/2 (even and odd parity) resonance for the same reaction as in Fig.2, as a function of beam momentum.

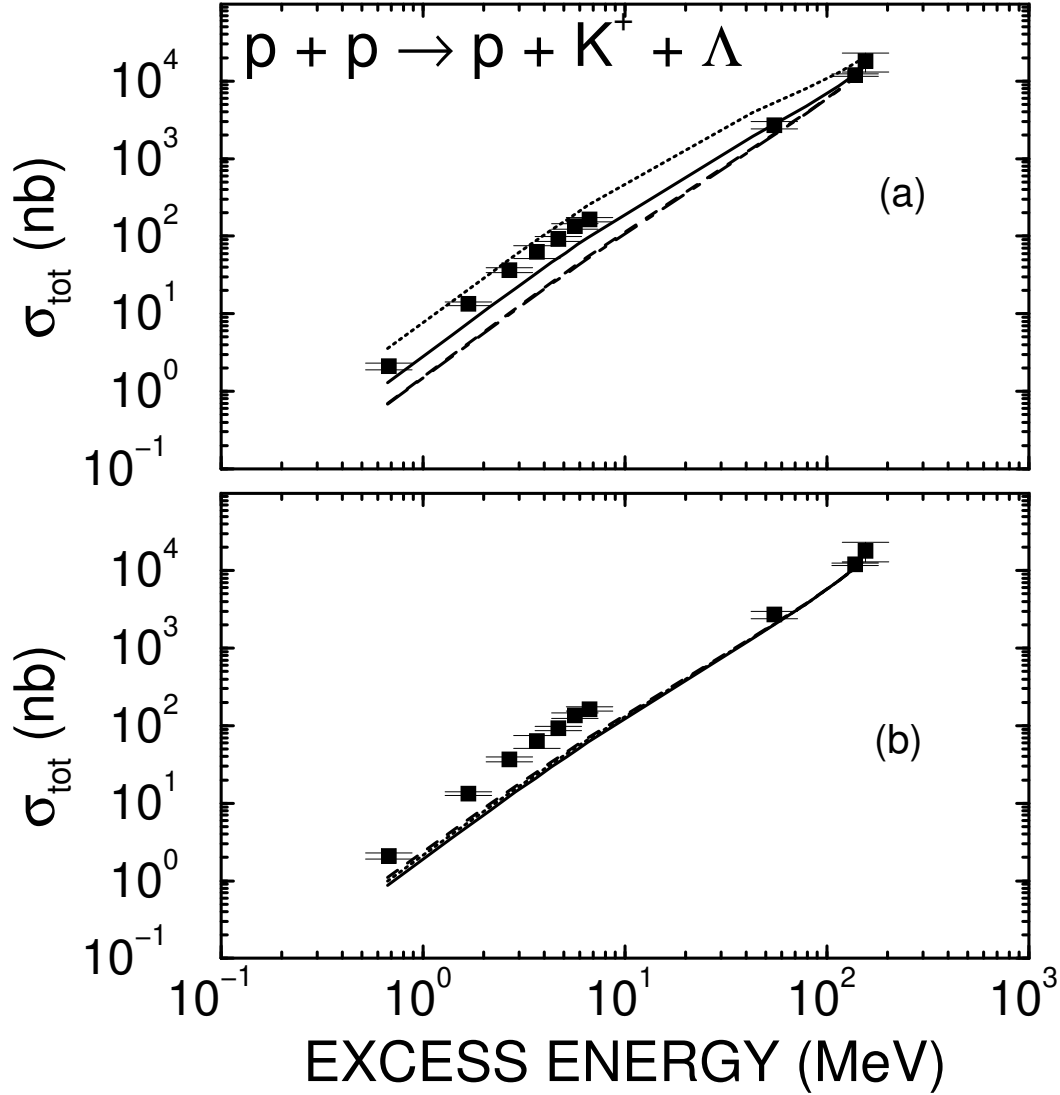


FIG. 5. The total cross section for the  $p + p \rightarrow p + K^+ + \Lambda$  reaction very close to the  $K^+$  production threshold as a function of the excess energy (defined in the text). The FSI effects are included by using the scattering length ( $a$ ) and effective range ( $r_0$ ) parameters for the  $K^+ - \Lambda$  and  $K^+ - p$  systems taken from the Feuster and Mosel [53] and those for the  $\Lambda - p$  system from the sets given by Jülich-Bonn [51] and Nijmegen [52] groups. In the upper part (a) results obtained with the  $\Lambda - p$  parameters of models A (solid line),  $\tilde{A}$  (dotted line), B (dashed line) and  $\tilde{B}$  (dashed-dotted line) of the former group are shown, while in the lower part (b) those of models D, F and NSC of the latter group are depicted. The results of the three models of the Nijmegen group are indistinguishable from each other. The experimental data is taken from [15,16]

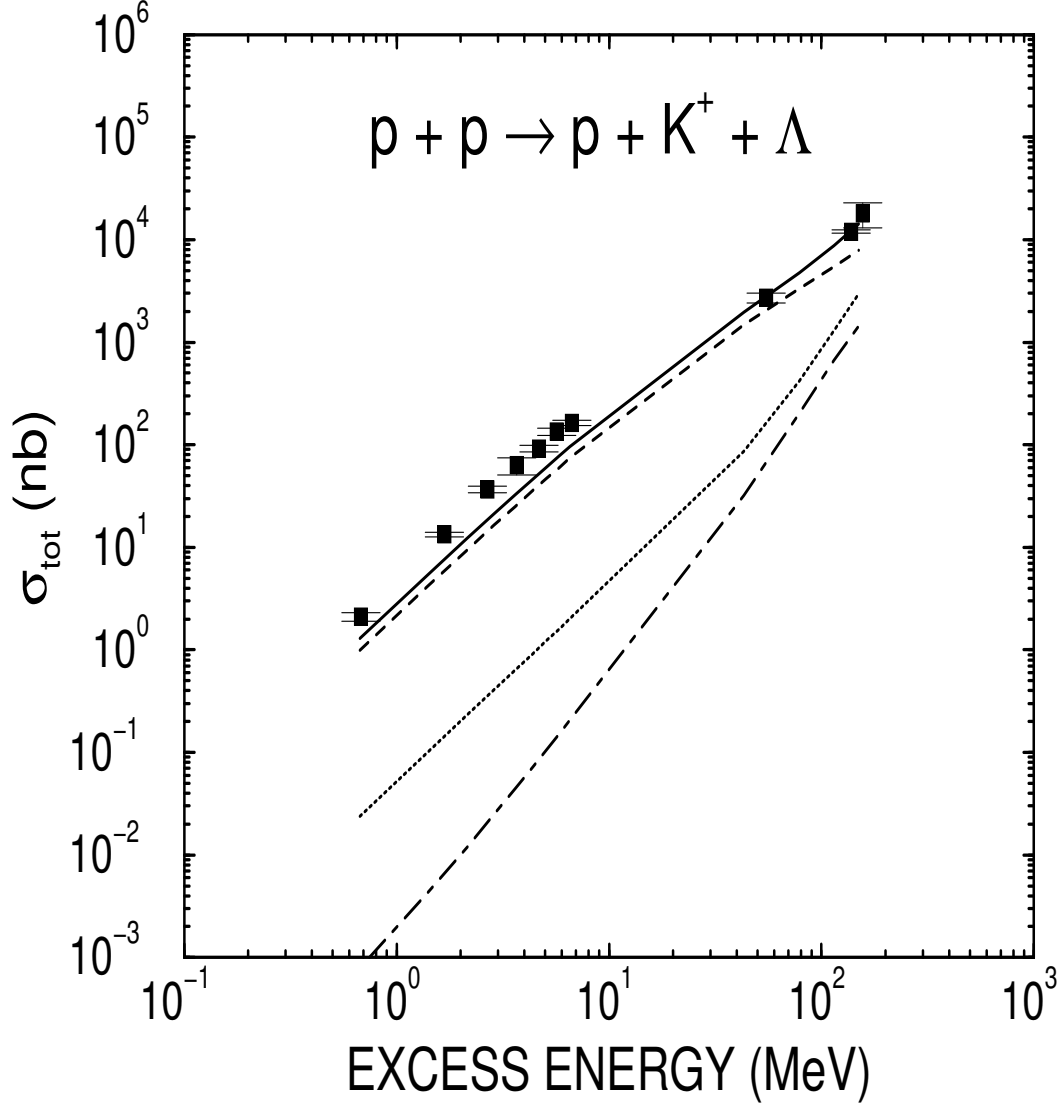


FIG. 6. Contributions of  $N^*(1710)$  (dotted line),  $N^*(1720)$  (dashed-dotted line) and  $N^*(1650)$  (dashed line) baryonic resonances to the total cross section for the same reaction as in Fig. 5, as a function of the excess energy. Their coherent sum is shown by the solid line. The FSI effects are included with  $a$  and  $r_0$  parameters of the  $K^+ - p$  and  $K^+ - \Lambda$  systems being the same as those in Fig. 5 and those for the  $\Lambda - p$  system being taken from the model A of the Jülich-Bonn group [51].



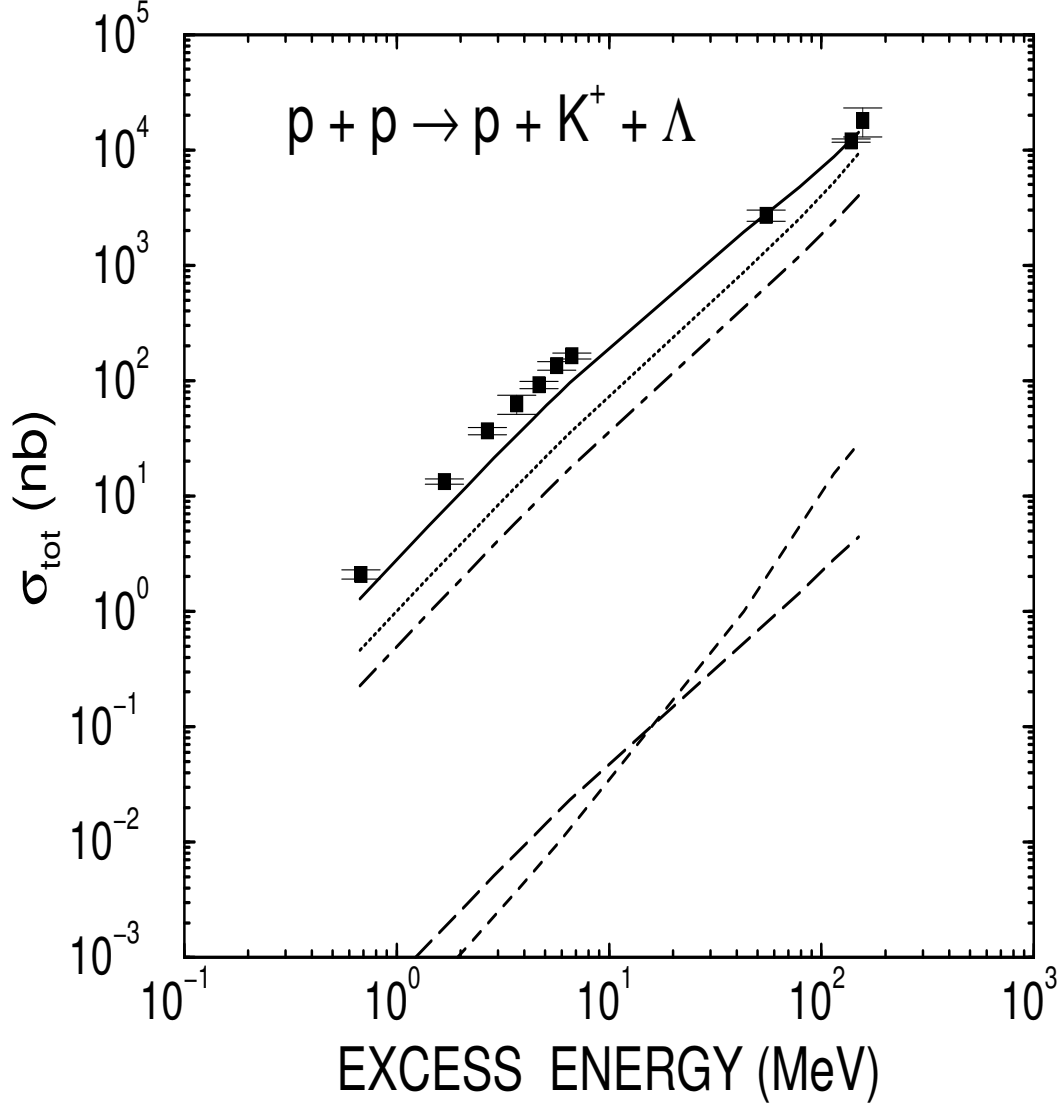


FIG. 7. Contributions of  $\pi$  (dotted line),  $\rho$  (dashed line),  $\omega$  (long-dashed line) and  $\sigma$  (dashed-dotted line) meson exchange processes to the total cross section for the same reaction as shown in Fig. 6, as a function of the excess energy. Their coherent sum is shown by the solid line. The FSI effects are included in the same way as in Fig. 6.